



Contents lists available at ScienceDirect

Journal of King Saud University – Science

journal homepage: [www.sciencedirect.com](http://www.sciencedirect.com)

Original article

# Heat-assisted sol–gel synthesis of $\text{TiO}_2$ nanoparticles structural, morphological and optical analysis for self-cleaning application

V.T. Lukong, K.O. Ukoba, T.C. Jen\*

University of Johannesburg, Auckland Park Campus, South Africa

## ARTICLE INFO

### Article history:

Received 13 May 2021

Revised 31 October 2021

Accepted 29 November 2021

Available online 2 December 2021

### Keywords:

 $\text{TiO}_2$ 

Nanoparticle

Sol–gel

Heat-assisted

Self-cleaning

## ABSTRACT

This study synthesized  $\text{TiO}_2$  nanoparticles using the sol–gel method assisted by heat from Titanium (IV) Isopropoxide. Samples were calcined at 400, 600, and 800 °C, and studied for self-cleaning application. The nanoparticles were characterized using X-ray diffraction (XRD), Scanning electron microscopy (SEM), transmission electron microscopy (TEM), Raman spectroscopy, and UV–vis spectroscopy. A self-cleaning application test was also performed using methylene blue dye as a form of contaminant. The  $\text{TiO}_2$  nanoparticles showed improved crystallinity with increased calcination temperature and experienced a phase transformation from anatase to rutile after 800 °C calcination. Crystallite size ranged from 5.11 to 24.97 nm for anatase and 15.85 to 24.72 nm for the rutile from the XRD result. Raman spectra showed increased peak intensities with an increase in calcination temperature. The grain size distribution from TEM analysis revealed the particle size with the uniform count at 400 °C and 800 °C than at 600 °C. The bandgap for direct transition was evaluated to be 3.07 eV. The self-cleaning test confirmed that the  $\text{TiO}_2$  nanoparticles would be effective in self-cleaning applications. The sample that was calcined at 600 °C displayed the highest self-cleaning ability.

© 2021 The Authors. Published by Elsevier B.V. on behalf of King Saud University. This is an open access article under the CC BY-NC-ND license (<http://creativecommons.org/licenses/by-nc-nd/4.0/>).

## 1. Introduction

Self-cleaning is the competence of a surface to rebuff all contaminants without external assistance. Any surface can self-clean if enriched with self-cleaning materials and its contact angle with water droplets regulated (Liu and Jiang, 2012). Materials with self-cleaning properties have found application in textiles (Pakdel et al., 2013), window glass surfaces (Cedillo-González et al., 2020), solar panels (Sakhuja et al., 2014), and water purification (Wang et al., 2020). A self-cleaning mechanism is engineered to be hydrophilic or hydrophobic. The choice of Self-cleaning materials is determined by low cost, durability, chemical and mechanical stability, anti-icing, non-toxicity, and anti-corrosiveness (Guldin et al., 2013). Titanium dioxide ( $\text{TiO}_2$ ), as a material, possess most of these properties (Astaneh et al., 2019).

$\text{TiO}_2$  self-cleaning capabilities prevent blight and defacement resulting from soiling effects on surfaces because it is highly efficient in photo catalyzing dirt in sunlight (Sarver et al., 2013). It naturally occurs in three distinct crystal anatomies (anatase, rutile, and brookite).  $\text{TiO}_2$  application is influenced by its morphology, grain size, and crystal phase (Gupta and Tripathi, 2011). The bandgap of  $\text{TiO}_2$  in the rutile crystal structure is 3.00 eV and is thermally stable. For the anatase and brookite crystal structure, the band gaps are 3.21 and 3.13 eV, respectively, and are thermally unstable (Mutuma et al., 2015). The rutile phase has been extensively applied in a thin film. At the same time, the anatase is employed mostly in photocatalysis and dye-sensitized solar cells due to its effective charge transfer characteristic (Vickers, 2017).  $\text{TiO}_2$  phases are obtained by controlling set process parameters. The benefits of using nanostructured  $\text{TiO}_2$  particles is that it quickly decomposes organic compounds and fosters the dissemination of water on the surface to accomplish its self-cleaning cycle (Somasundaram and Kumaravel, 2019). This is possible due to high-energy compactness and quick charge and discharge frequency (Malik et al., 2012).

Enormous research work has been undertaken with  $\text{TiO}_2$  nano-material (Nakata and Fujishima, 2012), and it is often synthesized by the wet chemical technique (Sagadevan, 2013), hydrothermal (Manjunath et al., 2018), the sol–gel (Behnajady et al., 2011), or

\* Corresponding author.

E-mail addresses: [ltakwa@live.co.uk](mailto:ltakwa@live.co.uk) (V.T. Lukong), [tjen@uj.ac.za](mailto:tjen@uj.ac.za) (T.C. Jen).

Peer review under responsibility of King Saud University.



Production and hosting by Elsevier

### Abbreviations

Np	Nanoparticles
SC	Self-cleaning

SILAR methods (Nkele et al., 2020). Nwankwo et al. (Nwankwo et al., 2019) successfully synthesized TiO<sub>2</sub> nanoparticles for photocatalytic application using the wet chemical method. However, the wet chemical method and the hydrothermal technique are somewhat complicated and not widespread due to the different chemicals involved and the specific control. Sol-gel synthesis of TiO<sub>2</sub> nanoparticles is achieved through hydrolysis and condensation of alkoxide of metals, which eventually progress to metal oxides (Yahaya et al., 2015). However, the hydrolysis process must be critically optimized by supervising the temperature at which it takes place. The molarity of the alkoxide and the acidic content also need control to achieve a homogeneous solution (Hanaor and Sorrell, 2011). The different phases of TiO<sub>2</sub> nanoparticles can be obtained or maintained by controlling their temperature (Sawant and Kale, 2020).

Sol-gel synthesis merits include simplicity, low cost, ease of control, and capability to mass-produce nano-scaled particles with extensive surface areas. However, this process has certain limitations, such as loose dispersal of particle proportions and particle clustering. Often surfactants are used to achieve better crystal structures, uniformity, and proportionate distribution of the particles (Kokare et al., 2018). But surfactants are not cheap and not readily available. This study focused on a better temperature-controlled process to obtain consistent and nanocrystalline TiO<sub>2</sub> nanoparticles to reduce cost. The as-prepared TiO<sub>2</sub> nanoparticles are then tested for self-cleaning application.

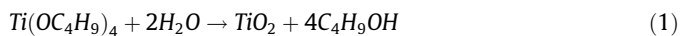
## 2. Experimental procedure

### 2.1. Chemicals

All chemicals used in this work and their sources are listed in Table 1

### 2.2. Synthesis of TiO<sub>2</sub> nanoparticles

All obtained chemicals were of analytical grades. The chemical reaction is shown in Equation (1).



Titanium (IV) Isopropoxide 97 % was dissolved in 99.9 % ethanol in a proportion of 1:5 while stirring. After 30 min, acid stock prepared by combining nitric acid with water in a 1: 50 ratio was added to the solution drop by drop while stirring at 500 rpm with a magnetic stirrer. The mixture was further stirred for 2 h at 60 °C for proper hydrolysis. After that, dried in an oven for 24 h at 100 °C

**Table 1**

List of materials, their origins, and purpose.

Material	Source	Purpose
Titanium (IV) Isopropoxide 97%	Sigma-Aldrich Germany	As the precursor of TiO <sub>2</sub>
Ethanol 99.9 %	Merck chemicals SA	As the sol-gel solvent
Nitric acid 70 % reagent	Sigma-Aldrich USA	As stabilizing agent
Deionized water	Merck chemicals SA	As sol-hydrolyzing agent

to form TiO<sub>2</sub> particles. The obtained TiO<sub>2</sub> nanoparticles were calcined at 400, 600, and 800 °C for 2 h for temperature optimization. Fig. 1 shows the synthesis process.

### 2.3. Characterization

The TiO<sub>2</sub> nanoparticles were characterized for crystal structure using an X-ray diffractometer (XPRT-PRO). The morphologies and elemental composition were examined under the Scanning Electron Microscope (X-MAX VEGA3 TESCAN), JEOL JEM 2100 80 T X-MAX for TEM analysis, and Energy Dispersive X-ray (EDX) Aztec Spectrometer (Oxford Instruments). The grain size was analyzed using ImageJ software. The optical properties were studied in 300 to 1000 nm wavelengths using a UV-2450 (SHIMADZU) spectrophotometer. Raman spectroscopy using theros-scientific DXR2 SmartRaman, class 1 Laser Product with 532 nm filter, and the self-cleaning test was performed by degrading methylene blue (MB) dye under UV-lamp irradiation (UV EQUIP T5 BLB 40 W and 40 cm in length) for two hours. The test tube was 10 cm deep and mounted 5 cm below the UV lamp throughout the test. The TiO<sub>2</sub> catalyst was separated using photovoltaic DF-L 0.22 μm filters, and the methylene blue concentrations were analyzed using a UV-2450 (SHIMADZU) spectrophotometer.

## 3. Results and discussion

### 3.1. Morphology analysis

The Morphologies of the TiO<sub>2</sub> nanoparticles were studied using SEM, TEM, and EDX. Fig. 2 shows the SEM micrographs and elemental compositions of the prepared TiO<sub>2</sub> nanoparticles after the calculations. The SEM images revealed cloudy oval-shaped particles with rough hierarchical structures and agglomeration. As the calcination temperatures increased, the particles increasingly became loose and well exposed in surface area. The result agreed with that obtained by Kokare et al. (2018). The well-exposed surface is desired in the self-cleaning application as it improves absorption. The EDX analysis revealed Titanium (Ti) and Oxygen (O) were the only elements present in higher weight percentages, with no impurity after calcination at 600 and 800 °C, thus confirming purification with heat-assistance.

Fig. 3 shows TEM images of the TiO<sub>2</sub> nanoparticles at 100 nm magnification for the different calcination temperatures alongside the grain size and the Gaussian distribution function using ImageJ software. The nanoparticles appeared in continuous chains, having long pear-shaped anatomies with visible dark spots. The grain size increased with increasing calcination temperature, with values of 4.59 10.24 and 23.69 nm<sup>2</sup> at 400, 600, and 800 °C, respectively.

The area distribution plot revealed that the particle size had a uniform count at 400 and 800 °C than 600 °C. This could be attributed to the unstable nature of the anatase phase at 600 °C. The fickle nature of the well crystalline anatase phase makes it more photocatalytic and is suitable for the self-cleaning application of TiO<sub>2</sub> (Choudhury and Choudhury, 2013).

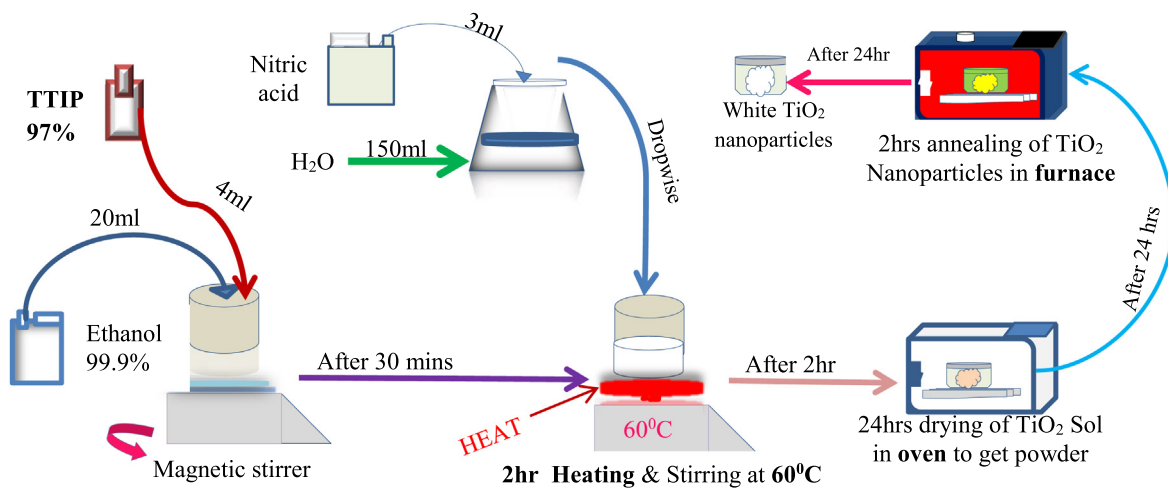


Fig. 1. Illustration of TiO<sub>2</sub> fabrication steps using heat-assisted sol-gel process.

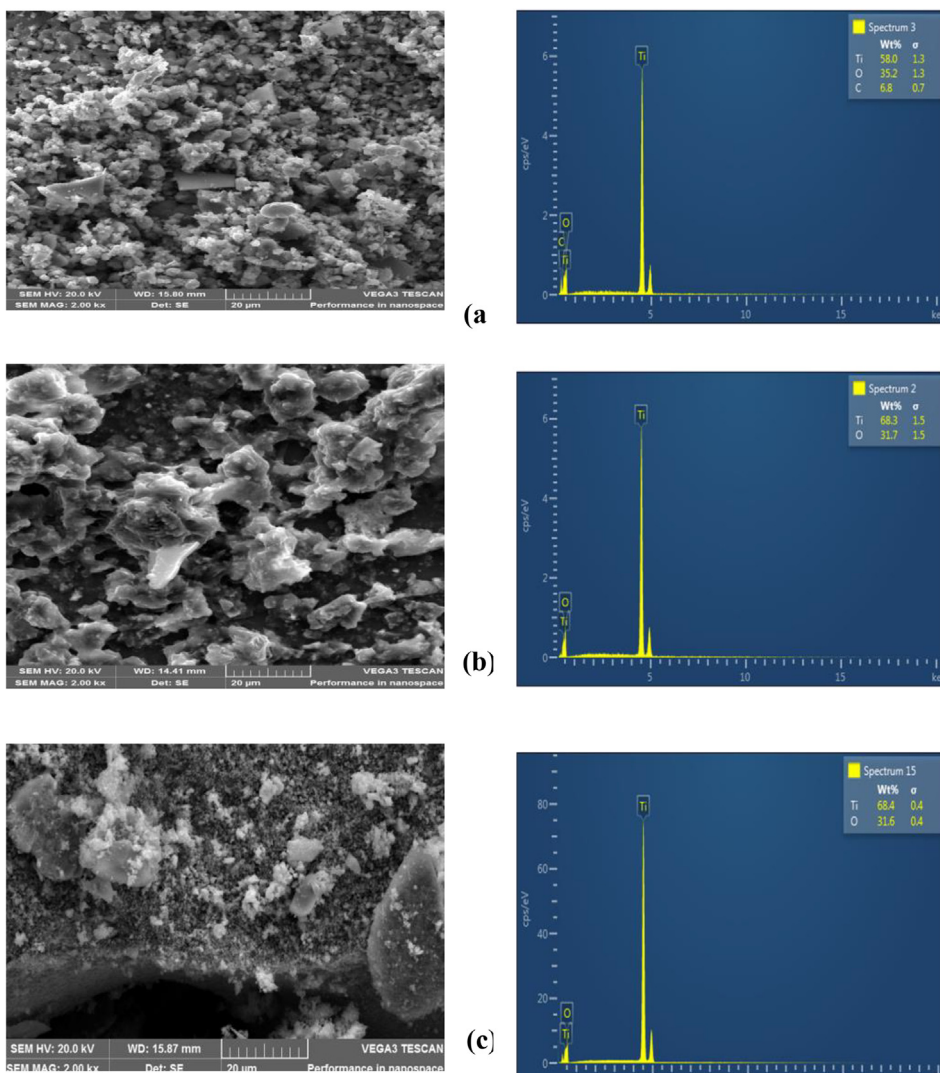


Fig. 2. SEM images and EDX analysis of the TiO<sub>2</sub> nanoparticles calcined at (a), 400 °C, (b) 600 °C, and (c) 800 °C.

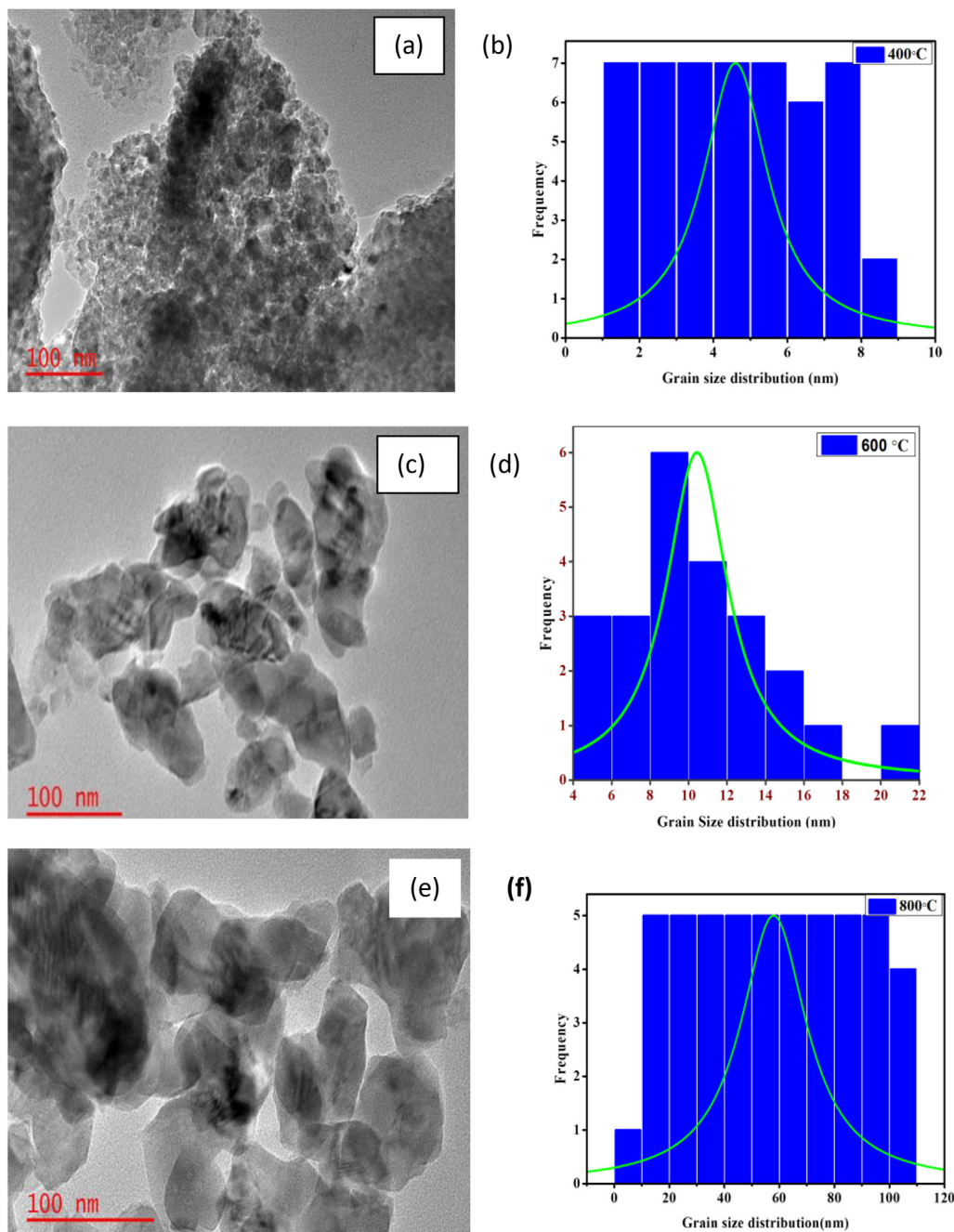


Fig. 3. TEM images, with the grain size distribution and Gaussian peak function for TiO<sub>2</sub> particles calcined at (a) 400 °C, (b) 600 °C and (c) 800 °C.

### 3.2. Structural analysis

The synthesized TiO<sub>2</sub> nanoparticles' structural analysis was studied using XRD and Raman spectroscopy. Fig. 4 shows the XRD patterns of TiO<sub>2</sub> nanoparticles after calcination at 400, 600, and 800 °C. The peaks revealed crystallinity improving with an increase in calcination temperature. The solid rutile peaks appearing after annealing at 800 °C indicates that phase transformation from anatase to rutile has occurred. The sample calcined at 600 °C displayed the most prominent anatase peak, which appeared at 2θ equals 25.32° and corresponding to miller index A (101). The most crystalline anatase phase was obtained at 600 °C while that of rutile was at 800 °C. The long calcination time contributed to the multi-crystalline nature of the nanoparticles after being heat-treated at 600 and 800-°C, due to grain boundaries

elimination and improved crystallinity (Valério and Morelhao, 2019). The patterns for 800 °C revealed the most substantial rutile peak at 27.44°, corresponding to *hkl* plane R(110) and matching ICDD card 01-072-4821.

The Debye-Scherrer formula (Chauhan et al., 2012) in Equation (2) was used to determine the average crystallite size.

$$D = \frac{k\lambda}{\beta \cos \theta} \tag{2}$$

With β representing full width at half maximum (FWHM) in Radian, λ is the wavelength (nm), θ is Bragg's diffraction angle, and shape constant k is 0.94.

Equations (3) and (4) were used to obtain the distance between parallel atomic planes d and the dislocation density, δ.

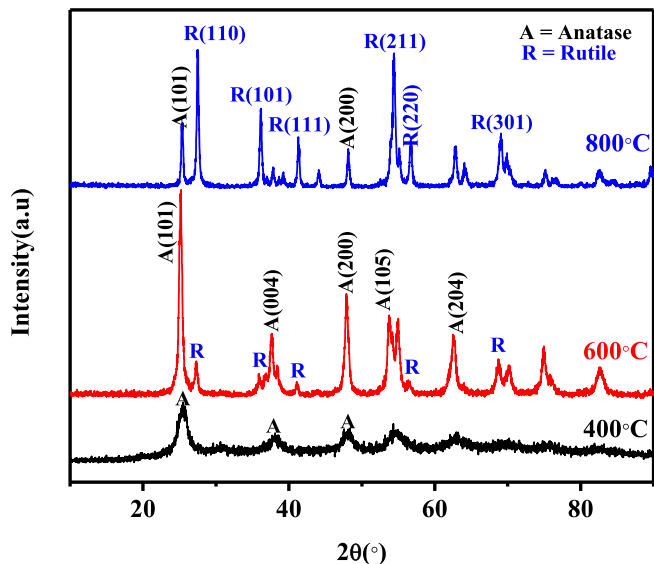


Fig. 4. XRD patterns of TiO<sub>2</sub> nanoparticles calcined at 400 °C, 600 °C, and 800 °C.

$$d = \frac{\lambda}{2 \sin \theta} \tag{3}$$

$$\delta = \frac{1}{D^2} \tag{4}$$

The values of the micro strains within the nanoparticles were computed using Equation (5)

$$\varepsilon = \beta / 4 \tan \theta \tag{5}$$

The lattice constants were calculated using Equation (6) (Pratheepa and Lawrence, 2018) and closely approximated the referenced JCPDS card. A(200) and A(004) were used as legends for the anatase phase and R(002) for the rutile

$$\frac{1}{d^2} = \frac{h^2 + k^2}{a^2} + \frac{l^2}{c^2} \tag{6}$$

In Table 2, the values computed for the lattice constants (a & c) of the TiO<sub>2</sub> nanoparticles for the anatase and the rutile phase are listed for the different calcination temperatures, alongside the crystallite size and other structural parameters.

For anatase, the average crystallite size was 10.48 nm, and for rutile, 20.29 nm, showing more nanostructure than bulk counterparts (Danish et al., 2014). This result affirms grain size obtained using TEM analysis. Enhanced crystal anatase structures offer a large surface area that absorbs solar energy per particle, making it more photocatalytic and suitable for self-cleaning. In addition, well crystalline structures have few crystal defects, implying a high surface-to-volume ratio that minimizes electron-hole recombination rate. More increased annealing temperature also causes phase transition from anatase to rutile. The rutile phase is very stable and less photocatalytic as compared to the anatase phase

Table 2

The TiO<sub>2</sub> nanoparticles crystallite size and other crystal parameters obtained at different calcination temperatures.

Calcination Temperature	Crystal phase	hkl	FWHM(°)	2θ(°)	D(nm <sup>2</sup> )	d(Å)	δ(nm <sup>-2</sup> )	ε × 10 <sup>-3</sup>	a (Å)	c (Å)
400 °C	Anatase	101	1.6644	25.45	5.11	3.4970	0.0383	32.1600	3.0774	9.4480
600 °C	Anatase	101	0.5509	25.16	15.76	3.5367	0.0040	10.7714	3.7934	9.5110
600 °C	Rutile	110	0.5387	27.33	15.85	3.2606	0.0040	9.6679	4.7756	5.3712
800 °C	Anatase	101	0.3406	25.32	24.97	3.5147	0.0016	6.6161	3.6454	9.9314
800 °C	Rutile	110	0.3455	27.44	24.72	3.2478	0.0016	6.1748	4.0259	2.6859

(Zhang and Li, 2020). Fig. 5 shows standard Raman spectra from 50 to 1200 cm<sup>-1</sup> observed for the TiO<sub>2</sub> nanoparticles after calcination at different temperatures. The spectra bands confirmed the six Raman modes for anatase TiO<sub>2</sub> that occurred around 145.51, 197.50, 396.50, 515.72, and 640.21 cm<sup>-1</sup>, corresponding to E<sub>g</sub>, B<sub>1g</sub>, A<sub>1g</sub> + B<sub>1g</sub>, and E<sub>g</sub>. The spectra confirm the XRD result of increasing crystallinity with an increase in calcination temperature (León et al., 2017). This is shown in the significant increases in Raman peak intensities as calcination temperature increases. The broadening of the TiO<sub>2</sub> peaks for particles calcined at 600 and 800 °C confirms crystallite size improvement and phase transformation associated with higher temperatures (Rahmati Ali Abad et al., 2020). Fig. 5 (b) shows a zoomed portion of the dual anatase peak and reveals a shift to higher wavenumber and broadening peaks at 600 and 800 °C calcination. This could be influenced by either charge excitation dissemination within the particles, increased crystallite size, or deformation in morphology (Peiró et al., 2001).

### 3.3. Optical studies

Fig. 6 shows the UV-vis spectroscopy result of the prepared TiO<sub>2</sub> nanoparticles for the sample calcined at 600 °C. The optical bandgap of the nanoparticle was obtained from the Tauc plot against incident light using Equation (7).

$$(\alpha h\nu)^n = K(h\nu - E_g) \tag{7}$$

where hv is the incident photon energy, α is the absorption coefficient, K being an energy-independent constant. E<sub>g</sub> is the optical bandgap value of the nanoparticle, and n is a value dependent on the nature of transition (n = 2 for direct allowed transition). Fig. 6 (a) shows that the TiO<sub>2</sub> nanoparticles calcined at 600 °C displayed high absorption in the visible light spectrum. High absorbance is characteristic of anatase TiO<sub>2</sub> due to more valence electrons holes for light absorption and is suitable for self-cleaning. No interference was observed. The TiO<sub>2</sub> particles at 600 were mainly anatase representing improved crystallinity due to the heat treatment. The transmittance spectral in Fig. 6(b) confirms about 85% of transmissions in the visible light region. The direct bandgap, evaluated by extending a straight line from the straight-line section of the curve of (αhv)<sup>n</sup> versus (hv) to intersect the x-axis, was 3.07 eV. as shown in Fig. 6 (c). This low bandgap value encourages high photocatalytic and self-cleaning activity due increase in absorption.

### 3.4. Self-cleaning application test

The TiO<sub>2</sub> nanoparticle self-cleaning ability was evaluated using the nanoparticle as a catalyst to degrade methylene blue (MB) dye under UV irradiation. 50 mg of TiO<sub>2</sub> nanoparticles was dissolved in 100 ml of 10 ppm MB for the photocatalytic degradation test. Fig. 7 (a) gives MB concentration drops with time. Maximum peaks at all concentrations were observed around the wavelength of 663 nm. The TiO<sub>2</sub> nanoparticles degraded the methylene blue dye effectively under UV-lamp illumination from 0 to 120mins. Fig. 7(b)

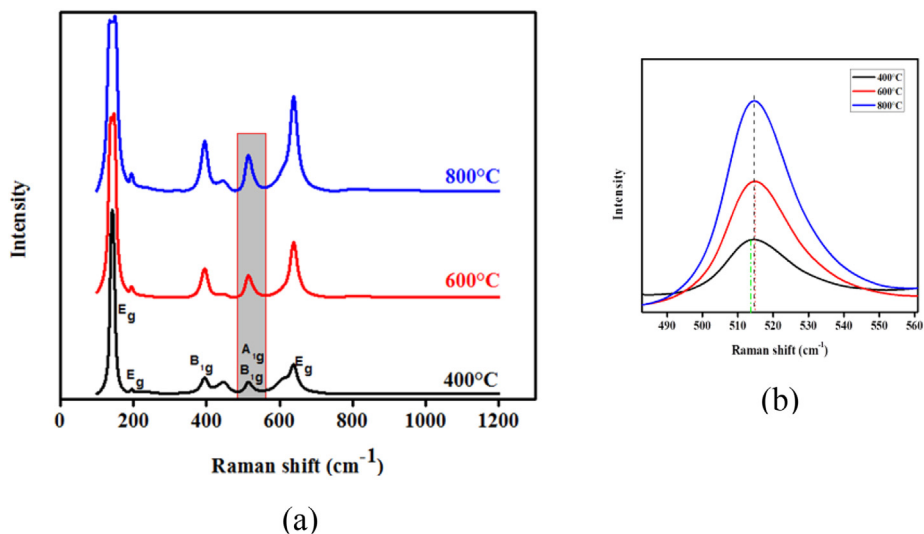


Fig. 5. Raman spectra of the TiO<sub>2</sub> nanoparticles (a) after calcination at 400, 600, and 800 °C (b) Exact peak position at 515.72 cm<sup>-1</sup> showing shift to higher wavenumber.

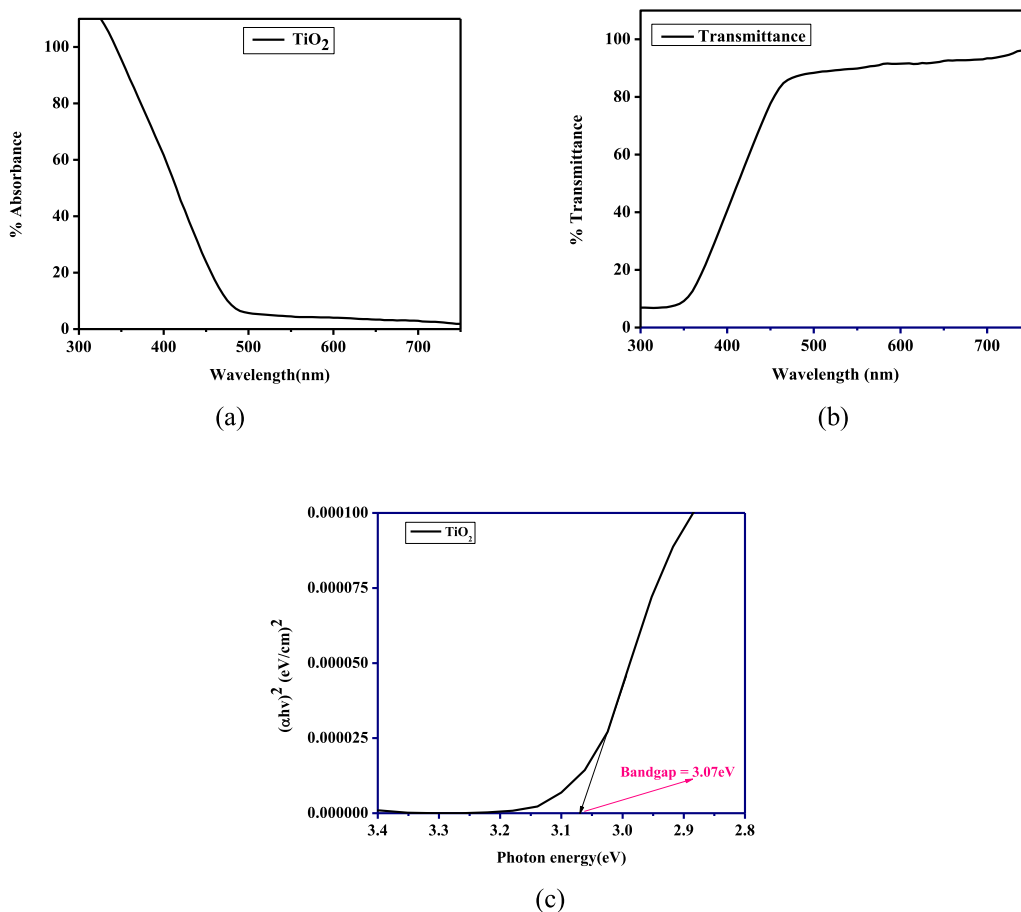


Fig. 6. (a) Absorbance spectral, (b) Transmittance spectral, and (c) Tauc plot against incident energy.

shows the percentage depletion of MB by the nanoparticles evaluated from the plot of absorbance efficiency versus time under UV-lamp. At the highest time of 120 min, almost 90% of the MB were degraded by the TiO<sub>2</sub> nanoparticles as effective self-cleaning material. This effective photocatalytic activity stems from the increasing active sites of the catalyst. The degradation rate constant for a first-order reaction was obtained from a

plot of  $\ln(C_t/C_0)$  against time as shown in Fig. 7(c) using Langmuir-Hinshelwood relation as expressed in Equation (8)

$$\ln(C_t/C_0)^{1/4} - Kt$$

where  $C_t$  indicates MB concentration at time  $t$ ,  $C_0$  is the initial concentration of MB under UV irradiation, and  $k$  is the rate constant.

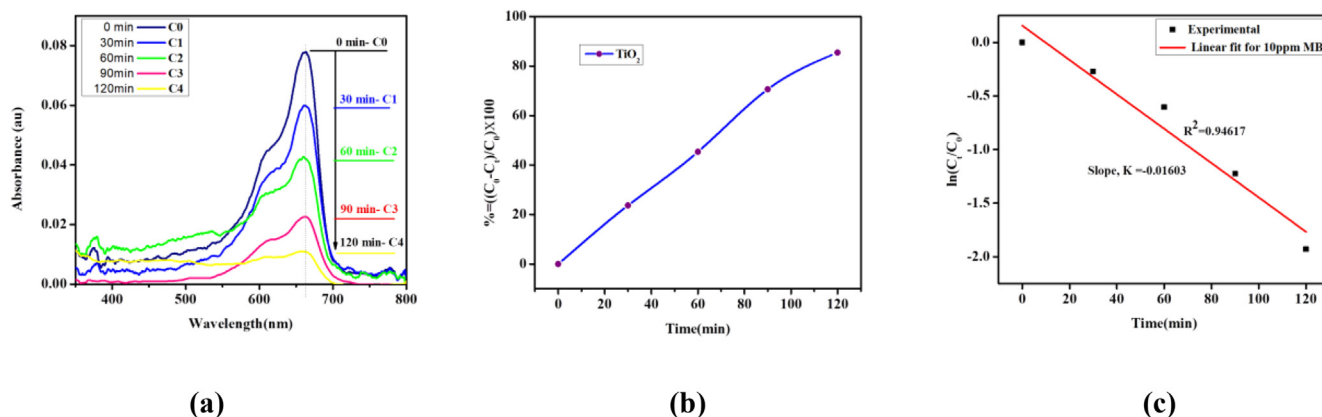


Fig. 7. Self-cleaning test (a) Evolution of MB concentrations versus irradiation time of UV-light. (b) Percentage degradation versus time, and (c)  $\ln(C_t/C_0)$  versus time of MB degradation.

The slope of a linearly fitted plot of  $\ln(C_t/C_0)$  vs time gave the value of  $k$  to be  $0.01603 \text{ min}^{-1}$  for implying higher photodegradation rates with increased dosage, like that obtained by Prabakaran and Pillay (2019) after doping  $\text{TiO}_2$  with ZnO. This again indicates that the prepared  $\text{TiO}_2$  is pure and of high quality.

#### 4. Conclusion

A simple heat-assisted sol-gel process was used to synthesize  $\text{TiO}_2$  nanoparticles for self-cleaning application. Synthesized particles were calcined at  $400^\circ\text{C}$ ,  $600^\circ\text{C}$ , and  $800^\circ\text{C}$  for temperature optimization and characterized using SEM, TEM, Raman, XRD, and UV-vis spectroscopy analysis. SEM analysis revealed oval-shaped and well-exposed morphologies that encourage high absorption. The grain size from TEM analysis and the crystallite size from XRD patterns showed an increase in size and crystallinity with the calcination temperature. The average crystallite size was  $10.48 \text{ nm}$  for anatase and  $20.29 \text{ nm}$  for the rutile phase. Raman spectral analysis showed a significant increase in peak intensity with an increase in calcination temperature. The bandgap was evaluated to be  $3.07 \text{ eV}$  for direct allowed transition. The general observation is that increasing the annealing temperature improved the photocatalytic properties and thus the self-cleaning ability of the  $\text{TiO}_2$  nanoparticles. However, at a higher calcination temperature of  $800^\circ\text{C}$ , complete phase transformation to rutile is achieved. This causes a drop-down in the self-cleaning function because the rutile phase is very stable and thus less photocatalytic. Therefore, increasing calcination temperature to a maximum of  $600^\circ\text{C}$  is recommended for  $\text{TiO}_2$  nanoparticles synthesis for self-cleaning applications.

#### Declaration of Competing Interest

The authors declare that they have no known competing financial interests or personal relationships that could have appeared to influence the work reported in this paper.

#### Acknowledgment

The authors appreciate the funding of NRF and URC of the University of Johannesburg, South Africa.

#### References

Astaneh, S.H., Jursich, G., Sukotjo, C., Takoudis, C.G., 2019. Surface and subsurface film growth of titanium dioxide on polydimethylsiloxane by atomic layer deposition. *Appl. Surf. Sci.* 493, 779–786.

- Behnajady, M.A., Eskandarloo, H., Modirshahla, N., Shokri, M., 2011. Investigation of the effect of sol-gel synthesis variables on structural and photocatalytic properties of  $\text{TiO}_2$  nanoparticles. *Desalination* 278 (1–3), 10–17.
- Cedillo-González, E.I., Hernández-López, J.M., Ruiz-Valdés, J.J., Barbieri, V., Siligardi, C., 2020. Self-cleaning  $\text{TiO}_2$  coatings for building materials: The influence of morphology and humidity in the stain removal performance. *Constr. Build. Mater.* 237, 117692. <https://doi.org/10.1016/j.conbuildmat.2019.117692>.
- Chauhan, R., Kumar, A., Chaudhary, R.P., 2012. Structural and optical characterization of Zn doped  $\text{TiO}_2$  nanoparticles prepared by sol-gel method. *J. Sol-Gel Sci. Technol.* 61 (3), 585–591.
- Choudhury, B., Choudhury, A., 2013. Local structure modification and phase transformation of  $\text{TiO}_2$  nanoparticles initiated by oxygen defects, grain size, and annealing temperature. *Int. Nano Lett.* 3 (1), 1–9.
- Danish, R., Ahmed, F., Koo, B.H., 2014. Rapid synthesis of high surface area anatase Titanium Oxide quantum dots. *Ceram. Int.* 40 (8), 12675–12680.
- Guldin, S., Kohn, P., Stefik, M., Song, J., Divitini, G., Ecarla, F., Ducati, C., Wiesner, U., Steiner, U., 2013. Self-cleaning antireflective optical coatings. *Nano Lett.* 13 (11), 5329–5335.
- Gupta, S.M., Tripathi, M., 2011. A review of  $\text{TiO}_2$  nanoparticles. *Chin. Sci. Bull.* 56 (16), 1639–1657.
- Hanaor, D.A.H., Sorrell, C.C., 2011. Review of the anatase to rutile phase transformation. *J. Mater. Sci.* 46 (4), 855–874.
- Kokare, A.M., Sutar, R.S., Deshmukh, S.G., Xing, R., Liu, S. and Lathe, S.S., 2018, May. ODS-modified  $\text{TiO}_2$  nanoparticles for the preparation of self-cleaning superhydrophobic coating. In *AIP Conference Proceedings* (Vol. 1953, No. 1, p. 100068). AIP Publishing LLC
- León, A., Reuquen, P., Garín, C., Segura, R., Vargas, P., Zapata, P., Orihuela, P.A., 2017. FTIR and Raman characterization of  $\text{TiO}_2$  nanoparticles coated with polyethylene glycol as carrier for 2-methoxyestradiol. *Appl. Sci.* 7 (1), 49.
- Liu, K., Jiang, L., 2012. Bio-inspired self-cleaning surfaces. *Annu. Rev. Mater. Res.* 42 (1), 231–263.
- Malik, M.A., Wani, M.Y., Hashim, M.A., 2012. Micro emulsion method: A novel route to synthesize organic and inorganic nanomaterials: 1st Nano Update. *Arabian J. Chem.* 5 (4), 397–417.
- Manjunath, K., Reddy Yadav, L.S., Jayalakshmi, T., Reddy, V., Rajanaika, H., Nagaraju, G., 2018. Ionic liquid assisted hydrothermal synthesis of  $\text{TiO}_2$  nanoparticles: photocatalytic and antibacterial activity. *J. Mater. Res. Technol.* 7 (1), 7–13.
- Mutuma, B.K., Shao, G.N., Kim, W.D., Kim, H.T., 2015. Sol-gel synthesis of mesoporous anatase-brookite and anatase-brookite-rutile  $\text{TiO}_2$  nanoparticles and their photocatalytic properties. *J. Colloid Interface Sci.* 442, 1–7.
- Nakata, K., Fujishima, A., 2012.  $\text{TiO}_2$  photocatalysis: Design and applications. *J. Photochem. Photobiol., C* 13 (3), 169–189.
- Nkele, A.C., Chime, U.K., Asogwa, L., Nwanya, A.C., Nwankwo, U., Ukoba, K., Jen, T.C., Maaza, M., Ezema, F.I., 2020. A study on titanium dioxide nanoparticles synthesized from titanium isopropoxide under SILAR-induced gel method: transition from anatase to rutile structure. *Inorg. Chem. Commun.* 112, 107705. <https://doi.org/10.1016/j.inoche.2019.107705>.
- Nwankwo, U., Bucher, R., Ekwealor, A.B.C., Khamlich, S., Maaza, M., Ezema, F.I., 2019. Synthesis and characterizations of rutile- $\text{TiO}_2$  nanoparticles derived from chitin for potential photocatalytic applications. *Vacuum* 161, 49–54.
- Pakdel, E., Daoud, W.A., Wang, X., 2013. Self-cleaning and superhydrophilic wool by  $\text{TiO}_2/\text{SiO}_2$  nanocomposite. *Appl. Surf. Sci.* 275, 397–402.
- Peiró, A.M., Peral, J., Domingo, C., Domènech, X., Ayllón, J.A., 2001. Low-temperature deposition of  $\text{TiO}_2$  thin films with photocatalytic activity from colloidal anatase aqueous solutions. *Chem. Mater.* 13 (8), 2567–2573.
- Prabakaran, E., Pillay, K., 2019. Synthesis of N-doped ZnO nanoparticles with cabbage morphology as a catalyst for the efficient photocatalytic degradation of methylene blue under UV and visible light. *RSC Adv.* 9 (13), 7509–7535.
- Prathepa, M.I., Lawrence, M., 2018. X-ray diffraction analyses of titanium dioxide nanoparticles. *J. Sci. Res. Sci. Tec* 3, 83.

- Rahmati Ali Abad, M., Shayesteh, S.F., Shayesteh, H.F., 2020. Effect of Synthesis Conditions on the Structural, Photocatalytic, and Self-Cleaning Properties of TiO<sub>2</sub> Nanoparticles. *Phys. Solid State* 62 (1), 120–130.
- Sagadevan, S., 2013. Synthesis and electrical properties of TiO<sub>2</sub> nanoparticles using a wet chemical technique. *Am. J. Nano Res. Appl.* 1 (1), 27. <https://doi.org/10.11648/j.nano.20130101.16>.
- Sakhuja, M., Son, J., Yang, H., Bhatia, C.S., Danner, A.J., 2014. Outdoor performance and durability testing of antireflecting and self-cleaning glass for photovoltaic applications. *Sol. Energy* 110, 231–238.
- Sarver, T., Al-Qaraghuli, A., Kazmerski, L.L., 2013. A comprehensive review of the impact of dust on the use of solar energy: History, investigations, results, literature, and mitigation approaches. *Renew. Sustain. Energy Rev.* 22, 698–733.
- Sawant, J.P., Kale, R.B., 2020. Surfactant mediated TiO<sub>2</sub> photoanodes and Cu<sub>2</sub>ZnSnS<sub>4</sub> counter electrodes for high efficient dye sensitized solar cells. *Mater. Lett.* 265, 127407. <https://doi.org/10.1016/j.matlet.2020.127407>.
- Somasundaram, S., Kumaravel, V., 2019. Application of Nanoparticles for Self-Cleaning Surfaces. In: *Emerging Nanostructured Materials for Energy and Environmental Science*. Springer, Cham, pp. 471–498.
- Valério, A. and Morelhaio, S.L., 2019. Usage of Scherrer's formula in X-ray diffraction analysis of size distribution in systems of monocrystalline nanoparticles. *arXiv preprint arXiv:1911.00701*.
- Vickers, N.J., 2017. Animal communication: when i'm calling you, will you answer too? *Curr. Biol.* 27 (14), R713–R715.
- Wang, J., Wang, X., Zhao, S., Sun, B., Wang, Z., Wang, J., 2020. Robust superhydrophobic mesh coated by PANI/TiO<sub>2</sub> nanoclusters for oil/water separation with high flux, self-cleaning, photodegradation and anti-corrosion. *Sep. Purif. Technol.* 235, 116166. <https://doi.org/10.1016/j.seppur.2019.116166>.
- Yahaya, M.Z., Abdullah, M.Z., Mohamad, A.A., 2015. Centrifuge and storage precipitation of TiO<sub>2</sub> nanoparticles by the sol-gel method. *J. Alloy. Compd.* 651, 557–564.
- Zhang, Q., Li, C., 2020. High Temperature Stable Anatase Phase Titanium Dioxide Films Synthesized by Mist Chemical Vapor Deposition. *Nanomaterials* 10 (5), 911.